11-2020

Triboelectric energy harvester with large bandwidth under harmonic and random excitations

Alwathiqbellah Ibrahim
University of Texas at Tyler, aibrahim@uttyler.edu

Abdallah Ramini

Shahrzad Towfighian

Energy Reports 6 (2020) 2490–2502

Contents lists available at ScienceDirect

Energy Reports

journal homepage: www.elsevier.com/locate/egyr

Triboelectric energy harvester with large bandwidth under harmonic and random excitations

Alwathiqbellah Ibrahim [a,*], Abdallah Ramini [b], Shahrzad Towfighian [c]

[a] The University of Texas at Tyler, 3900 University Blvd., Tyler, TX 75799, United States of America
[b] Penn State Harrisburg, 777 W Harrisburg Pike, Middletown, PA 17057, United States of America
[c] Binghamton University, 4400 Vestal Parkway E., Binghamton, NY 13902, United States of America

ARTICLE INFO

Article history:
Received 16 March 2020
Received in revised form 2 September 2020
Accepted 4 September 2020
Available online xxxx

Keywords:
Triboelectric
Energy harvesting
Random
Impact model

ABSTRACT

This paper investigates an approach to impact vibration energy harvesting using a triboelectric mechanism under harmonic and random excitation. The harvester consists of a clamped–clamped beam with a stiff plate in the middle to realize the impact electrification process when subjected to external vibrations. The harvester uses stiffening in the clamped–clamped beam introduced by the impact between two triboelectric layers to increase the frequency bandwidth. A piecewise theoretical model is used to model the harvester for two scenarios of motions, before and after impact. The harvester is tested experimentally under different harmonic excitation to validate the theoretical model. The outcomes show a good agreement between both experimental and theoretical results. Higher bandwidth is achieved at a lower gap separation distance. The operating bandwidth of the energy harvester increased from 4.4 Hz to 17.8 Hz with an RMS output voltage level of 7 V and an output power density of 7 mW/m^2 at 1.4 g excitation level and 100 μm gap. The model is extended and validated experimentally under random excitation. The simulated power spectral densities are in good agreement with the experimental results.

1. Introduction

Mechanical vibrational energy harvesting has been given significant attention by researchers as a potential alternative power source. In recent years, the triboelectricity mechanism has demonstrated as a new alternative mechanism for energy harvesting (Fan et al., 2012; Wang, 2013; Wang and Wu, 2012). Because of several advantages, such as higher power output, low-cost materials, and a simple fabrication process, the triboelectric mechanism is considered one of the most efficient techniques for energy harvesting. In the triboelectric mechanism, contact electrification happens when two materials of different polarities contact and separate from each other. Zi et al. (2016), Wang et al. (2015), Yi et al. (2015), Zhou et al. (2014), Zeng et al. (2013), Zhang et al. (2014). The materials must have opposite tendencies to lose and gain electrons. Aluminum material tends to lose electrons when it meets another less positive triboelectric material such as Polydimethylsiloxane (PDMS) (Diaz and Felix-Navarro, 2004; Dhakar et al., 2016; Khan et al., 2017). PDMS has many useful characteristics, such as excellent elasticity and flexibility, surface malleability, biocompatibility, and easy fabrication. These properties of the PDMS make it attractive for using PDMS-based energy harvesters in many applications. The cyclic process of contact and separation creates an alternating current as the charges flow between the two triboelectric layers. The charge density is a function of multiple factors, such as the chemical properties of the materials and the micro-surface patterns that control the area of contact (Henniker, 1962). Surfaces with micro-patterns increase the contact area and enhance the conversion efficiency (Dhakar et al., 2015b; Jin et al., 2016).

Because of their narrow operating bandwidth, linear vibration-based energy harvesting devices are considered inefficient. Different types of nonlinearities are considered by researchers to increase the frequency bandwidth, such as magnetic (Mann and Sims, 2009; Erturk et al., 2009; Stanton et al., 2010, 2012; Bilgen et al., 2015; Ibrahim et al., 2016, 2017), and mechanical forces (Gammaitoni et al., 2009; Masana and Daqaq, 2011; Sneller et al., 2011; Sari et al., 2008; Mahmoud, 2010). Internal resonance (Yang and Towfighian, 2017), multiple cantilevers that have close natural frequencies (Al-Ashtari et al., 2013), and softening in springs (Nguyen and Halvorsen, 2011) are different approaches that broaden the operation frequency bandwidth. A bistable cantilever energy harvester with piezoelectric material under magnetic nonlinearity was demonstrated and found to improve operating frequency bandwidth (Stanton et al., 2010; Ibrahim et al., 2016, 2017). Impact vibration energy harvesting is an alternative approach used to increase the frequency

* Corresponding author.
E-mail address: aibrahim@uttyler.edu (A. Ibrahim).

https://doi.org/10.1016/j.egyr.2020.09.007

bandwidth (Dhakar et al., 2015a, 2014, 2015b; Niu et al., 2013; Soliman et al., 2009). However, among all these studies, no in-depth investigation was demonstrated regarding impact vibration triboelectric harvesters. One of the efficient studies in impact vibration harvesters is the work conducted by Mahmoud and Abdel-Rahman (Mahmoud, 2010). They investigate an impact vibration energy harvester based on electrostatic transduction. However, triboelectric transducers are more efficient than electrostatic ones because the material used in triboelectric devices can charge itself when subjected to impact from vibration sources.

Most of the studies reported above used a known harmonic base excitation form. However, most ambient vibrations are random. To understand the energy harvesting devices operating under random excitations, the ambient vibrations should be described with probability and random vibrations theories (Papoulis and Pillai, 2002). One of the first studies that considered energy harvesting under random vibrations was done by Lefeuvre et al. (2007). Halvorsen (2008) extracted a closed-form expression that reflects the amounts of energy harvested from a linear energy harvester using a random vibration theory. Adhikari et al. (2009) derived a mean power for piezoelectric vibration harvester subjected to a random base excitation signal with exact closed-form expressions using the method of random vibrations. The expression is provided for two different circuit connectivity, with and without an inductor. Litak et al. (2010) investigate a piezoelectric ferromagnetic cantilever beam energy harvester under random excitation. They induced bistability from two permanent magnets to improve the coupling to the electrical system and the performance of the energy harvester. A similar design was done by Ferrari et al. (2011). Blystad et al. (2010) investigated the effect of stoppers and power conversion circuitry on the performance of an energy harvester subject to harmonic and random excitation. Harmonic excitation was found to be promising at low and high excitation amplitudes under variable load resistance. On the other hand, the output power caused by random vibrations was found to be sensitive to stopper loss, which should be considered if this loss is to be minimized. However, those results are a numerical result, and no experimental validation was provided. Zhao and Erturk (2012) studied bimorph piezoelectric energy harvester configurations under random excitation. The effect of higher vibration modes is also investigated, and they found that lightly damped higher modes can alter the expected power curve under white noise excitation. A piezoelectric buckled beam vibration energy harvester is investigated theoretically and experimentally by Cottone et al. (2012). The piezoelectric beam shows higher output electric power when it is compressed than in the unbuckled case. A randomly excited bi-resonant cantilever-mass impact structure with attached polyvinylidene fluoride (PVDF) films based piezoelectric energy harvester (PPEH) was developed to enhance the bandwidth, Li et al. (2016a,b). A similar study was conducted under electrostatic coupling between the randomly excited bi-resonant cantilever-mass structure, Zhang et al. (2016). The electrostatic coupling results in broadening the bandwidth of the energy harvester. Electret-based micro energy harvester with a gap-closing mechanism investigated under low pressure to reduce the air damping and increases the Q-factor (Zhang et al., 2018; Guo et al., 2020). The bandwidth of the harvester is broadened by stacking two-devices, where their resonances found to be merged at higher excitation. A coupled system of electromagnetic and triboelectric transduction mechanisms was demonstrated in a rotational pendulum design of a hybridized generator (RPHG) (Guo et al., 2020). The system is tested under different external excitation to optimize the electrical output performance of the device. A hybrid energy harvester with a similar coupling mechanism was investigated with a nonlinear stiffness design to address widening bandwidth and to enhance the device performance (Gupta et al., 2017). For more information about combinations and other energy harvesting mechanisms, the reader can refer to Shi et al. (2019), Liu et al. (2018). However, the investigation of the triboelectric energy harvesters under random excitation remains missing in the literature.

Many small electronics and sensors are converting from being battery powered to self-powered. This conversion is done by harvesting biomechanical or ambient energies generated by human walking, heartbeats, machine vibration, and random vibrations from automobiles and wind. Triboelectric energy harvesting is a new and effective energy harvesting technique. This technique provides the necessary power for many small electronics that would not need battery or sensor replacement (Wang et al., 2017a), making it attractive for a wide range of applications in the automotive and bio-sectors. Also, it shows high performance at low frequencies, making it superior for biomedical applications to harvest energy produced by heart beating and respiratory motion (Zheng et al., 2016), human interaction (Dong et al., 2018; Yang et al., 2018), blood pressure (Liu et al., 2017; Li et al., 2014), and human movement for implantable and wearable devices (Chen et al., 2020; Wen et al., 2016). In transportation, there are many sources of wasted energy, such as vibration energy, wind energy, impact, etc. In the field of intelligent transportation systems (Ahmadian, 2008; Jin et al., 2017; Chen et al., 2015; Wang et al., 2017b; Li et al., 2018), the triboelectric mechanism is used as driver behavior monitoring (Meng et al., 2018), safety systems (Guo et al., 2018b), tire monitoring (Guo et al., 2018a), and emission monitoring (Shen et al., 2018).

Here, we focus on designing a PDMS triboelectric energy harvesting device capable of harvesting energy under various types of excitations. This harvester provides a solution to overcome the low energy density and the narrow operating bandwidth problems in energy harvesting devices. We fabricate a triboelectric energy harvester to convert harmonic and random mechanical vibrations into usable energy. PDMS microscale semi-cylindrical grooves are employed to increase the contact surface area, and hence to enhance the generated power. Also, we develop a theoretical piecewise model to understand the separation and contact motions. This energy harvester design shows the feasibility of the triboelectric transduction mechanism to convert mechanical energy into electrical energy. The mechanical energy is of the form of harmonic and random vibrations. The electrical energy might be used in powering microsensors.

The organization of this article is as follows: In Section 2, we discuss the triboelectric energy harvester design and configurations. We described the working mechanism in Section 3. In Section 4, we developed the theoretical model using a lumped parameter model approach and providing the experimental setup in Fig. 5. The harmonic and random analysis are explained in Sections 6 and 7, respectively, and finally, we end with conclusions in Section 8.

2. Device design and configuration

Fig. 1 shows the schematic of the proposed device using the triboelectric mechanism. The triboelectric energy harvester (TEH) comprises two parts: an upper Aluminum part and a lower PDMS part. The device is working based on the periodic contact and separating between its upper and lower parts. The Aluminum layer is engraved with semi-cylindrical patterns and serves as a mold for the polydimethylsiloxane (PDMS) layer. The molded PDMS, which has mirrored semi-cylindrical grooves, is placed on the thin, bottom Aluminum layer. The upper part is attached to a clamped–clamped polymer beam as a central mass. When the device is in operation, the clamped–clamped polymer beam

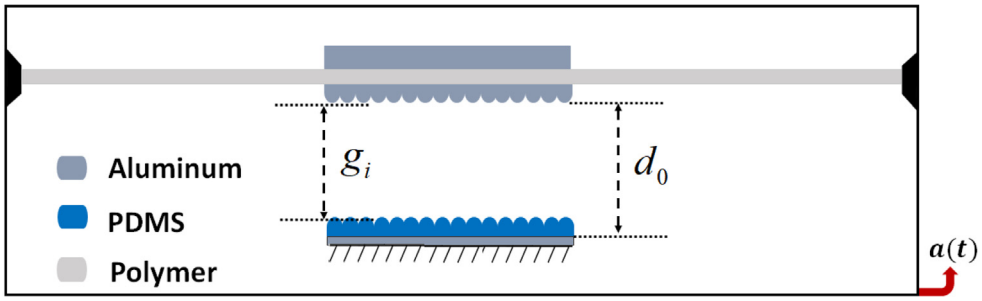

Fig. 1. Schematic for the triboelectric energy harvester.

Table 1
List of dimensions and structural parameters of the harvester parts.

Structural parameters	Value
Beam (l, w, h)	(15, 3.7, 0.1) cm
Center mass (l, w, h)	(5.2, 3.8, 0.5) cm
Mold (l, w, h)	(5.2, 3.7, 0.4) cm
Density of Aluminum	2700 kg/m^3
Density of Polymer	1220 kg/m^3

can vibrate, while the lower part remains fixed, as shown in Fig. 1. When the device is excited at the base with mechanical vibrations, the upper and lower parts undergo a periodic contact and separation movement. During the contacting-separating motion, both layers will be full of different charges, and hence alternating current is produced (Wang, 2013). The lower part will restrict the amplitude of the clamped–clamped beam motion, which results in the broadband behavior of the TEH (Soliman et al., 2008; Dhakar et al., 2013; Liu et al., 2012). Progressive Tool Co. of Endwell, NY, Progressive Tool Co Kernel Description (2015) grooved the semi-cylindrical micropatterns into the Aluminum layer. The semi-cylindrical micropatterns, Fig. 2(a), increase the contact area of the two surfaces, generating more power. The structural parameters for the triboelectric generator are in Table 1.

A (5.2 ×3.7× 0.4) cm Al mold with semi-cylindrical micropatterned grooves (Fig. 2a) is designed and machined by Progressive Tools (Progressive Tool Co Kernel Description, 2015). This Al mold is used to fabricate the PDMS layer and acts as the upper electrode in the energy harvester. The micropatterns increase the surface contact between the layers of the energy harvester. In the beginning, the Al mold is cleaned by immersion in distilled water for 10 minutes using Ultrasonicator. The water is replaced with acetone, and the process is repeated for another 10 minutes. Then, the cleaning with water is repeated one more time. The mold is dried using a Nitrogen gun. A 10 : 1 mass ratio of silicone elastomer base and a curing agent is mixed to achieve homogeneous mixture with a lot of air bubbles. After that, the mixture is vacuumed for an hour or more until all bubbles are removed. Next, the cleaned Al mold is treated with a SIH5841.0 agent to help in peeling off the PDMS later. After that, a piece of glass is placed on top of a heater, and the PDMS mixture is poured on it. Immediately, an edge of the AI mold with the micropatterns downward is embedded in the PDMS mixture, and the tilted mold is slowly flattened into the mixture to avoid trapping air bubbles, which would interact with the PDMS. Then, the mixture is baked at 80 °C for an hour and a half. After baking, the PDMS layer is peeled off from the Al mold yielding a thin layer with a semi-cylindrical reverse pattern, as shown in Fig. 2b. Later, this PDMS layer is bonded to a thin Al layer to create the lower electrode.

3. Energy harvester cycle of work

The cycle of work is shown for the triboelectric transduction mechanism in Fig. 3. Under no mechanical load, the generator's layers are separated by a spring-like restorative force from a cantilever beam with a center mass. In the beginning, the upper and lower layers are out of charges (Neutral), Fig. 3a. When the device is subjected to mechanical excitation, the beam starts to vibrate, and the two layers contact each other, Fig. 3b. When contact happens between the layers, and because Al material tends to lose electrons, while the PDMS layer tends to gain electrons, the Al layer will be positively charged while the PDMS will be entirely negatively charged. As the mechanical load becomes weak, the beam restoring force starts to separate the two layers. At this stage, a potential difference is induced between the two layers, and the current starts to flow from the upper Al layer toward the lower Al layer, as shown in Fig. 3c. This process continues until the full separation between the two layers occurs. The triboelectric and electrostatic charges are in equilibrium when complete separation happens, Fig. 3d. Continuity of the applied mechanical excitation results in moving of the two layers toward each other, and again the equilibrium between the two layers is disturbed. This disturbance makes the current flow in the other direction from the upper layer to the lower one, as shown in Fig. 3e. Then, the cycle repeats.

4. Theoretical model

The flexible clamped–clamped beam holds a center mass and vibrates under mechanical excitation, providing the contact and separation mechanism required for charge electrification generation. Here, the clamped–clamped beam is excited with two different types of signals using an electromagnetic shaker. Initially, the harvester is subjected to a harmonic vibration input signal, and then the harmonic signal is replaced by a random Gaussian white noise signal. For both cases, the harvester is modeled as a Single Degree of Freedom (SDOF) lumped parameter model with two scenarios: before and after impact, Fig. 4. The significant differences between the two situations are the stiffness and damping, which becomes more damped after the impact. An additional impact spring force with a stiffness of k_i is added to the mechanical stiffness k_{eq} when the upper electrode is in contact with the lower one in Fig. 4(b). The total forces acting on the upper electrode are shown in Fig. 4(c).

The upper and lower electrodes of the triboelectric generator are considered as a parallel plate capacitor. According to Fig. 4, the governing equations for the two scenarios (Mahmoud, 2010), are given by Eqs. (1) and (2). The definitions of the variables are listed in Table 2. For solving the system under harmonic

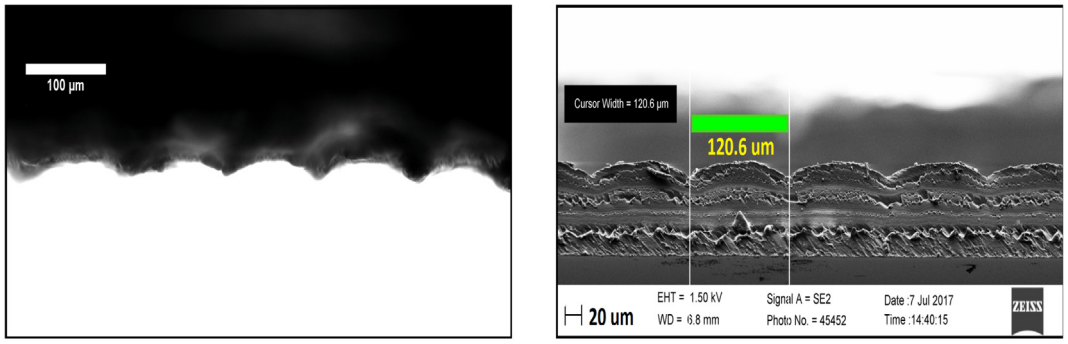

(a) (b)

Fig. 2. Upper and lower layers of the triboelectric generator (a) Aluminum mold. (b) SEM image for the PDMS layer.

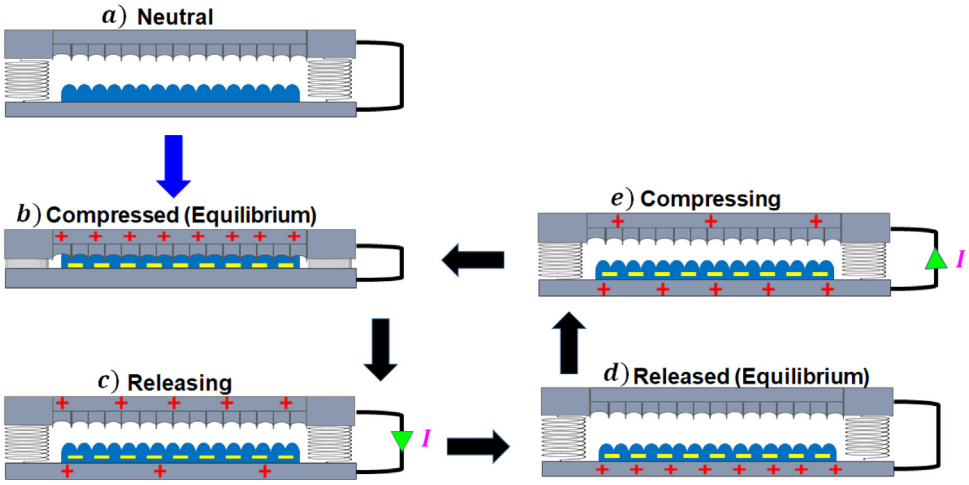

Fig. 3. Operating mechanism for the triboelectric energy harvester.

Table 2
The definitions for the variables used in the theoretical model.

Variable	Definition
m	The effective mass of the structure
$y(t)$	Relative displacement
c_m	Mechanical damping coefficient
$a(t)$	Base excitation
$q(t)$	Charges transferred
S	Total electrode area
ϵ_0	Vacuum permittivity $= 8.85 \times 10^{-12}$ F/m
ϵ_r	The dielectric constant for the PDMS
σ	Surface charge density
T	The thickness of the PDMS layer
g_i	The gap between the upper electrode and PDMS
δ	Maximum allowable penetration distance

excitation, we use the shooting method (Appendix). In contrast, numerical integration is used to address the system under random excitation using Mathematica software (Wolfram, 1987).

$$m\ddot{y}(t) = \begin{cases} -c_m\dot{y}(t) - k_{eq}y(t) + \frac{q^2(t)}{2\epsilon_r\epsilon_0 S} - ma, & y(t) < g_i \\ -c_i\dot{y}(t) - k_i y(t) - (k_{eq} - k_i)g_i - ma, & y(t) \geq g_i \end{cases} \quad (1)$$

$$\dot{q}(t) = -\frac{q(t)}{\epsilon_0 RS}\left(\frac{T}{\epsilon_r} + d_0 - y(t)\right) + \frac{\sigma}{\epsilon_0 R}(d_0 - y(t)) \quad (2)$$

5. Experimental setup

Fig. 5 shows the experimental setup used for testing the devices. We use an electromagnetic shaker to investigate the dynamics of the harvester experimentally under different types of excitation. LabView software (NI, 1976) is used to generate harmonic and random signals with a NI USB-6251 data acquisition board. The generated signal is amplified and sent to the electromagnetic shaker, which simulates low-frequency vibrations. To measure the provided acceleration, (352A24) an accelerometer from PCB Piezotronics with a sensitivity of 100 mV/g is placed on the shaker. The accelerometer signal and output voltage are sent back to the LabView software through the data acquisition board. A variable resistance box is used to control the resistance.

6. Harmonic analysis

The identified parameters of the energy harvester and some experimentally extracted parameters are summarized in Table 3. The gap between the two electrodes is measured with a blade metric feeler gauge, and the estimated gap value is corrected by matching the RMS output voltage from the model to the experimental output voltage. The remaining parameters (c_m, k_i, c_i) used in the simulation are extracted by curve fitting with the experimental results. According to these parameters, the fundamental natural frequency for the generator is found to be 20 Hz.

The optimal resistance matching the internal impedance of the harvester is estimated by varying the value of the resistance and measuring the changes in the voltage, current, and power outputs

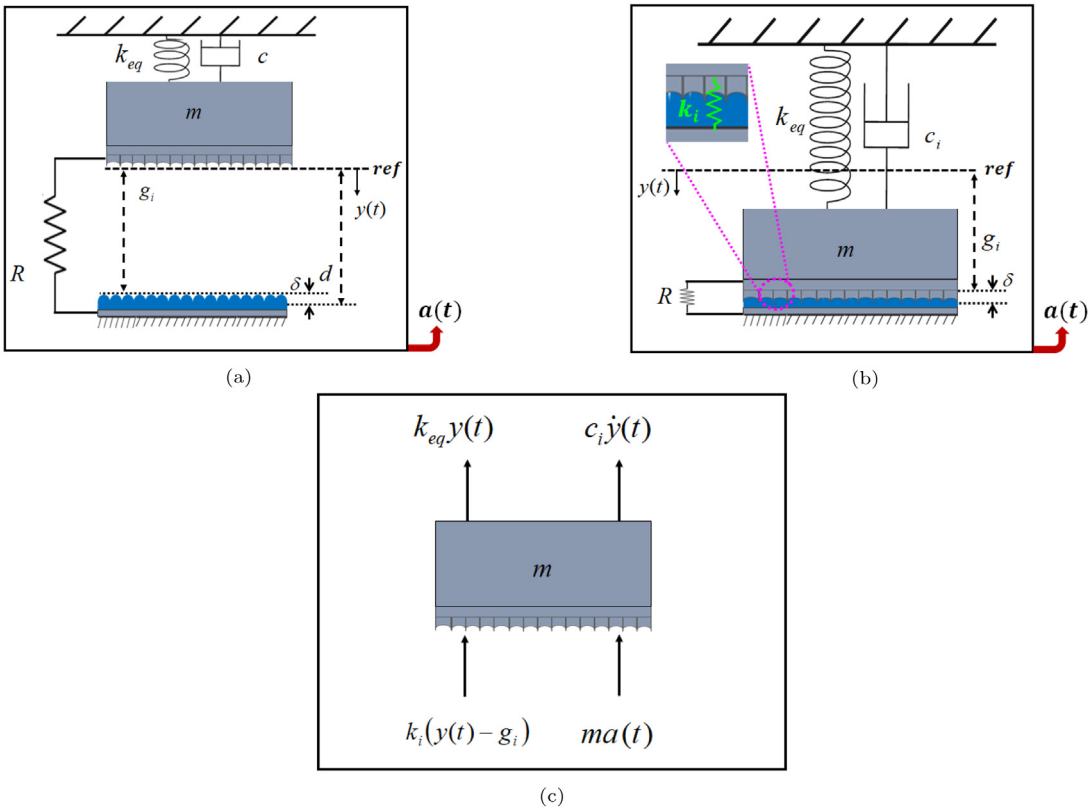

Fig. 4. SDOF system model (a) before impact; (b) at the onset of impact (zoomed in); (c) free body diagram during impact.

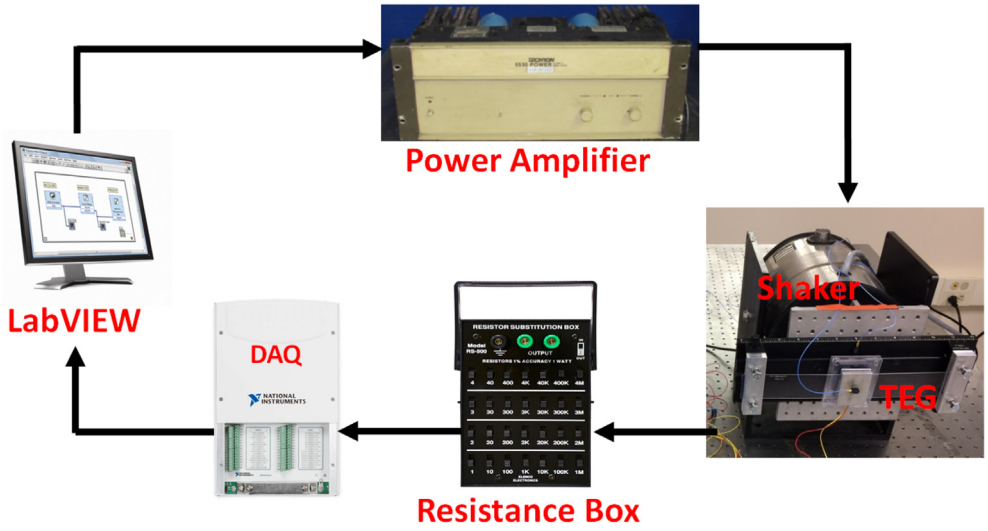

Fig. 5. Schematic for the experimental setup.

Table 3
Experimentally extracted parameters for the harvester.

Parameters		Value
Mechanical stiffness	k_{eq}	1056 N/m
Impact stiffness	k_i	12 k_{eq}
Mechanical damping coefficient	c_m	0.325 N.s/m
Effective beam mass	m_{eff}	0.00254 kg
Center mass	M	0.0480168 kg
Impact damping coefficient	c_i	200 c_m
Maximum penetration distance	δ	10 μm

at 0.5 g excitation level in Fig. 6. The Voltage–Current intersection and the power curves show optimal resistance of $R = 4$ MΩ.

The testing was conducted at different excitation levels for two different gaps. The output voltage, current, and power curves are shown for two different gaps of 100 μm, and 250 μm, with an optimal resistance of 4 MΩ, Fig. 7. The amplitudes values increase as the excitation levels increase and reach maximum values of 7.5 V, 1.7 μA, and 14 μW of voltage, current, and power, respectively, at 1.4 g. By comparing the results from the two gaps, the amplitudes values of the 250 μm gap are more substantial than of the 100 μm gap at low excitation levels. However, the 100 μm gap device operates in a much wider bandwidth than

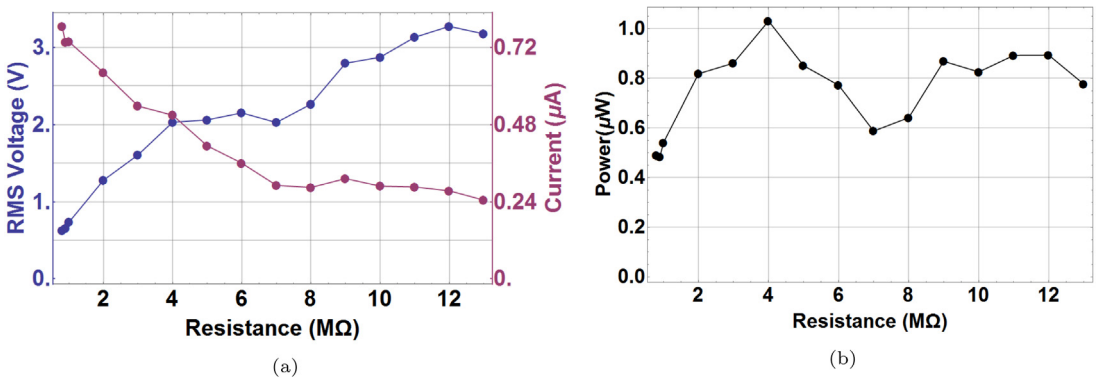

Fig. 6. Dependence of the voltage, current, and power outputs on the identified resistance at 0.5 g excitation and 25 Hz frequency with sine sweep signal (a) Voltage–Current dependence, (b) Power dependence.

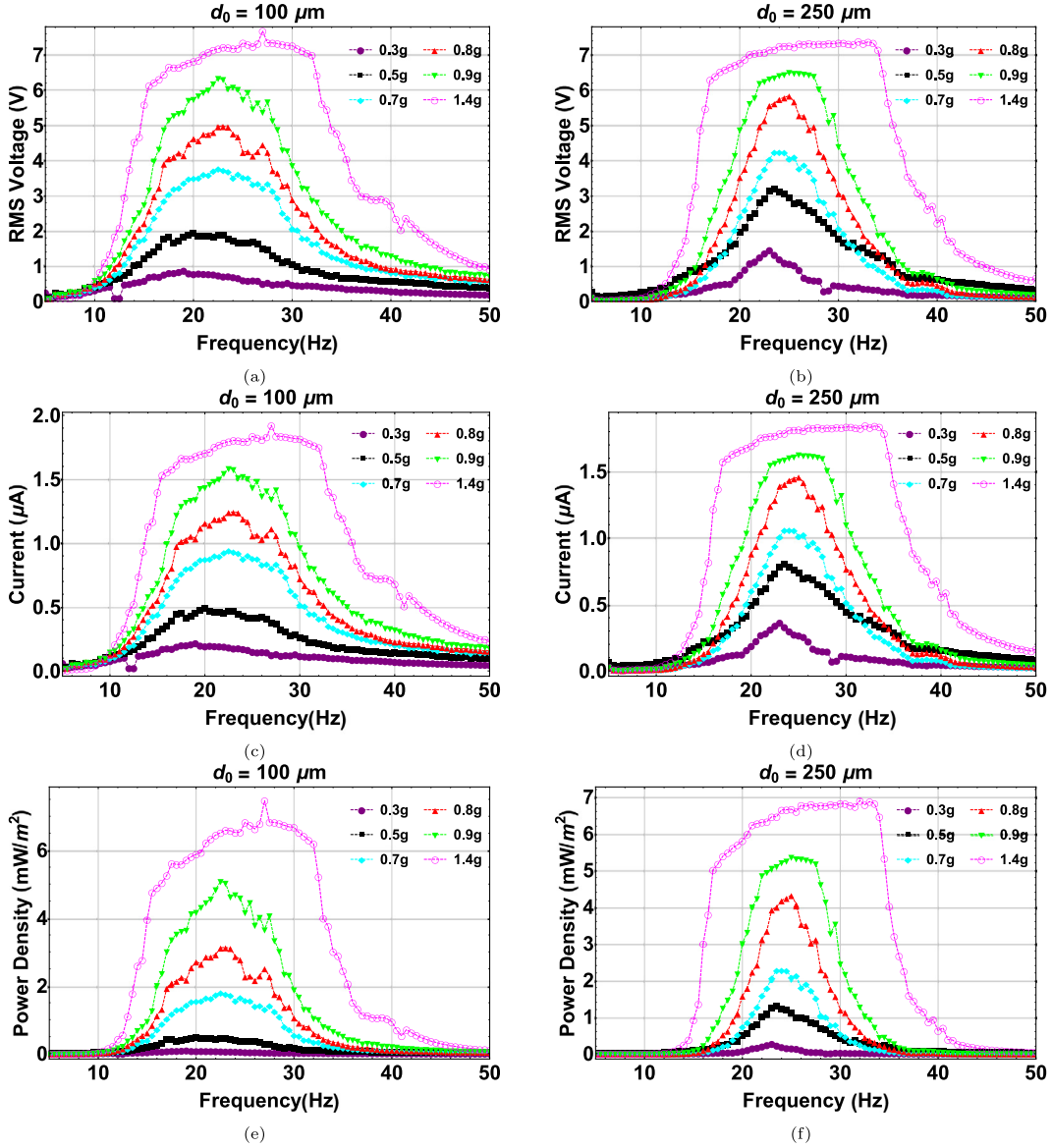

Fig. 7. Experimental response curves for the triboelectric generator at different excitation levels at the optimal resistance of $R = 4$ MΩ at two different separation gaps (a, b) RMS Voltage, (c, d) Current, (e, f) Power density.

the 250 μm gap device. The broader bandwidth can be related to the increasing number of collisions between the layers. The larger gap promotes increased linear momentum, which results in stronger impacts and better output.

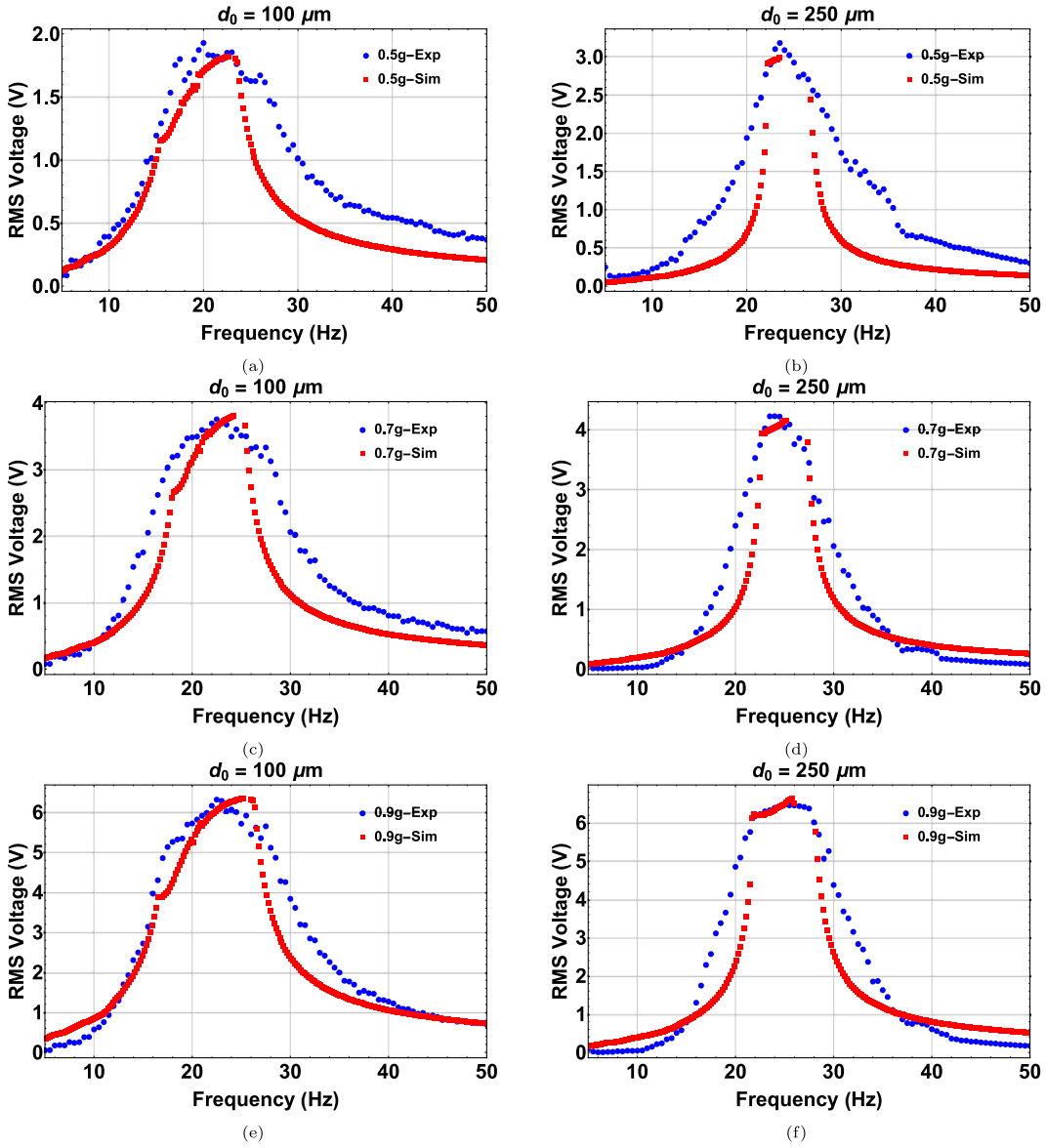

Fig. 8. Experimental and simulated voltage response at different excitation levels at different separation gaps with the following estimated surface charge densities (a) $\sigma = 4.5$ $\mu C/m^2$ (b) $\sigma = 4.5$ $\mu C/m^2$, (c) $\sigma = 7.5$ $\mu C/m^2$, (d) $\sigma = 7.0$ $\mu C/m^2$, (e) $\sigma = 11$ $\mu C/m^2$, (f) $\sigma = 10$ $\mu C/m^2$.

To verify our model, we simulate the response of the harvester for the 100 μm and 250 μm gaps, Fig. 8. The simulated results show a good agreement with the experimental results. We also notice that the values of the surface charge densities used to match the experimental results are lower for the 250 μm than those of 100 μm. Because a more extensive penetration occurs at smaller gaps, the surface charge density is more significant. However, this larger surface charge does not lead to a larger power output because the rates of change of the charge and power are lower at smaller gaps, according to Eq. (2). The corresponding output current and power are shown in Fig. 9 and Fig. 10, respectively.

Next, the gap between the two electrodes is varied experimentally, and the maximum output voltage is recorded for each difference, as shown in Fig. 11(a). The optimum gap based on the output voltage found to be around 300 μm. Similarly, the bandwidth for each gap is recorded, and the optimum bandwidth is observed to be for a lower gap of 150 μm, as shown in Fig. 11(b). This observation means that the larger power is obtained at the price of the bandwidth.

7. Random analysis

The dynamics of the energy harvester are investigated experimentally and theoretically under a Gaussian white noise excitation signal to validate our model under a random input signal. Here, the experimental Power Spectral Density (PSD) curves at different RMS Gaussian white noise excitation signals for a 100 μm gap are shown in Fig. 12(a). The PSD represents the distribution of a signal over a spectrum of frequencies. The output voltage increases by increasing the RMS values and increasing the gap between the two electrodes to 250 μm in Fig. 12(b) increases the amplitudes while the bandwidth gets narrow. This observation is consistent with the results of the harmonic excitation. To obtain the simulated PSD of the output voltage under random excitation, the base acceleration term in the system of

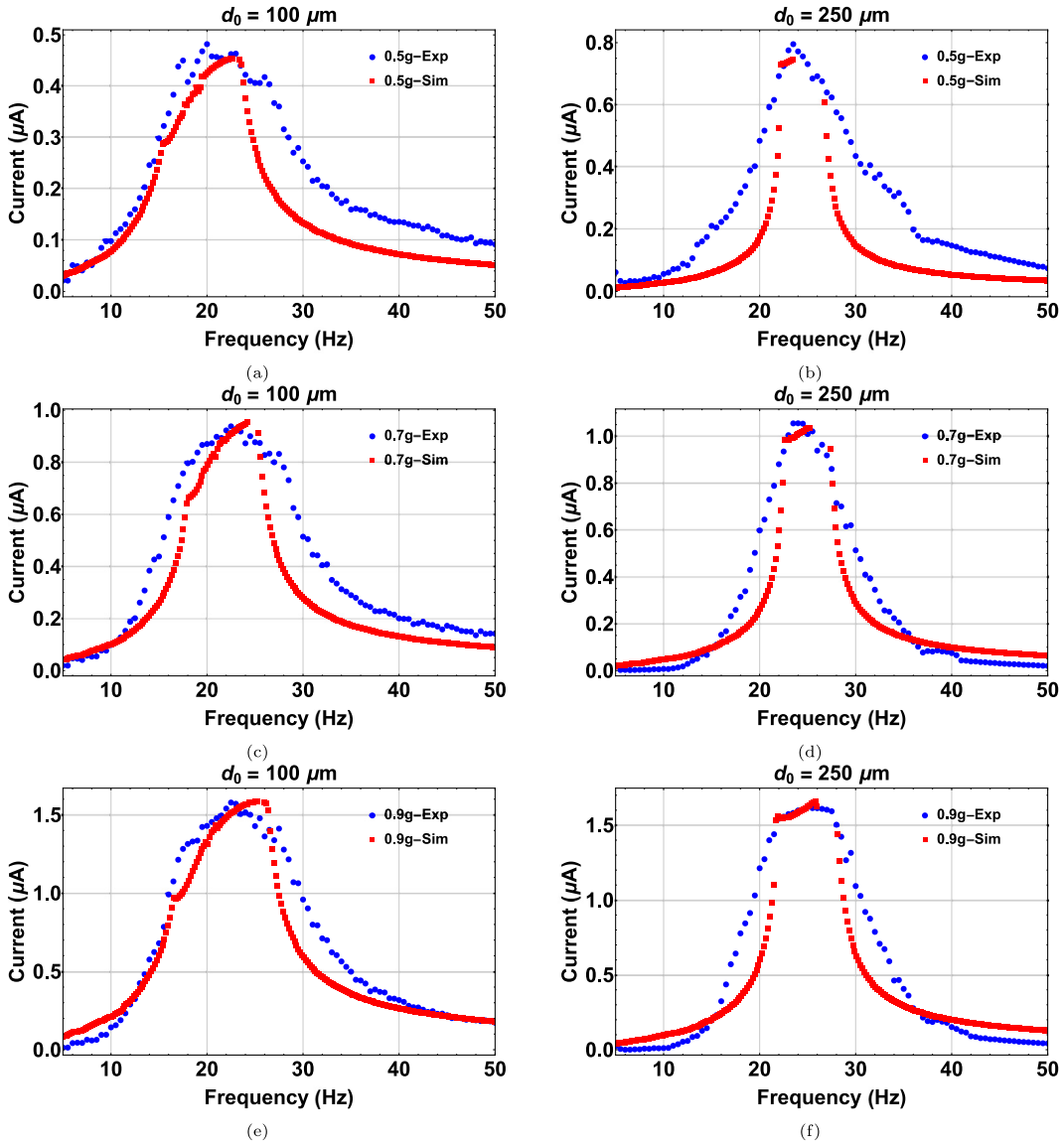

Fig. 9. Experimental and simulated current response at different excitation levels at different separation gaps with the following estimated surface charge densities (a) $\sigma = 5$ μC/m^2 (b) $\sigma = 4.5$ μC/m^2, (c) $\sigma = 8.5$ μC/m^2, (d) $\sigma = 7.0$ μC/m^2, (e) $\sigma = 12$ μC/m^2, (f) $\sigma = 10$ μC/m^2.

equations in Eq. (1) is replaced with a random Gaussian white noise signal, then the system is solved numerically to extract the voltage response. Then the PSD is calculated by applying a Fourier transform to the discrete voltage. To simulate the experimental conditions, we used the random signal from the experimental results as an excitation input in our model. Fig. 13 shows the experimental and simulated PSD curves. The simulated results in these figures are in excellent agreement with the experimental results. We assume the surface charge density to match the experimental results. However, the surface charge densities are considered very low compared to the harmonic results. This consideration is deemed to be acceptable because the input signal is random, and the contact between the two electrodes is less than the harmonic case.

Following the current development in the technology of triboelectric energy harvesters, it is possible to modify current sensors to be self-powered. In the biomedical sector, the triboelectric mechanism harvests energy from heartbeats, respiratory motion, activities of daily living, and blood pressure. In the automotive industry, the triboelectric device used to convert the position, thermal, gas, and pressure sensors into self-powered sensors. Possible applications for the current manuscript are harvesting the energy of random automotive motions to power sensors used to monitor driver habits in the automotive industry and of the low-frequency human walking activity to power and monitor implants in the biomedical sector.

We presented an impact vibration harvester that achieves a broader bandwidth by replacing the linear stiffness with a piecewise stiffness function. This impact harvester addresses the severe limitation of linear one whose narrow bandwidth causes low conversion efficiency as a small deviation from the natural frequency results in a significant output loss. Using this piecewise stiffness function, a larger amplitude is spread over a broader range of frequency, improving the conversion efficiency of mechanical vibration to electricity. Moreover, the analysis is extended to study the viability of the triboelectric energy harvesters for different applications that subjected to random excitation.

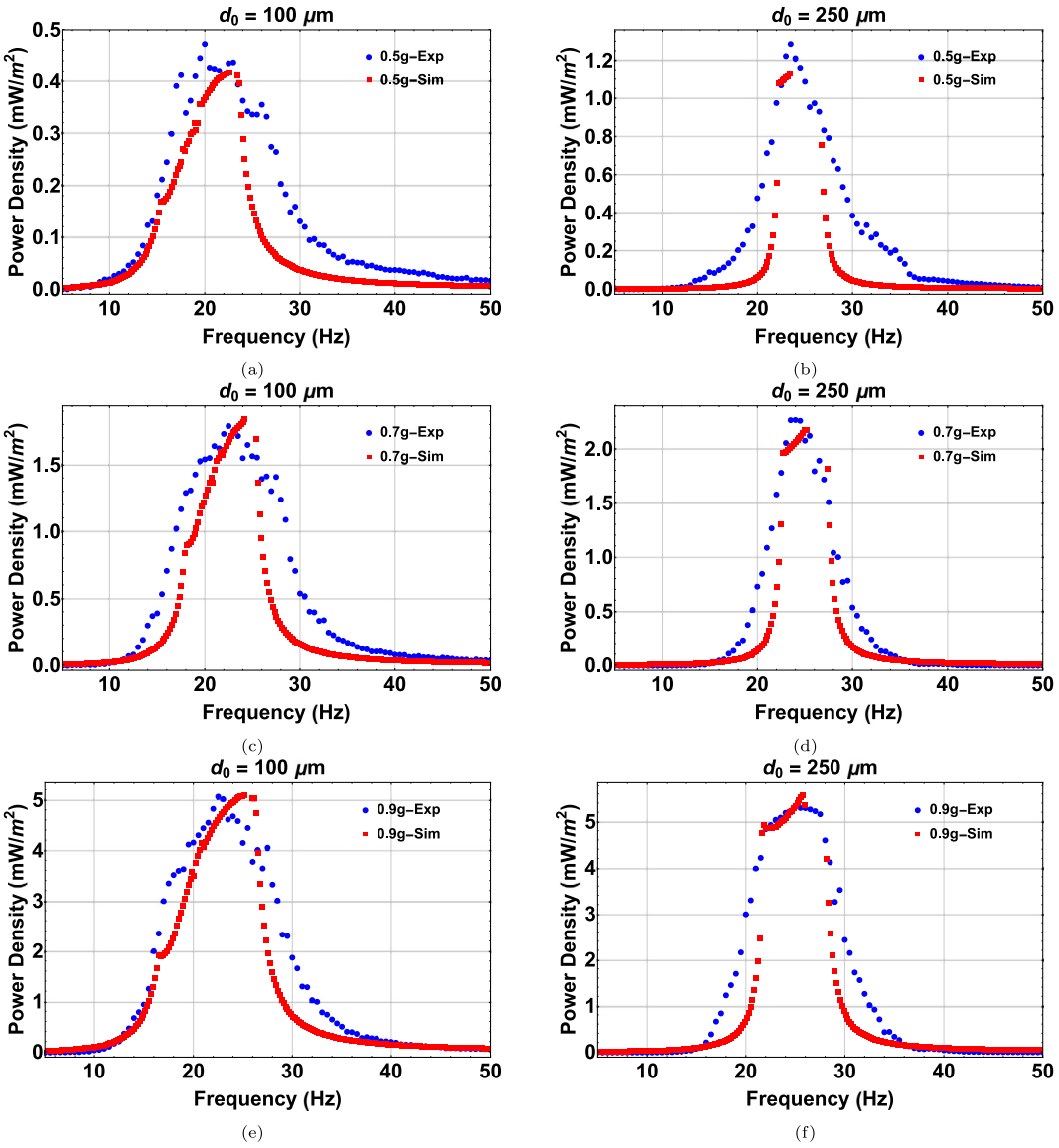

Fig. 10. Experimental and simulated power density response at different excitation levels at different separation gaps with the following estimated surface charge densities (a) $\sigma = 5$ μC/m^2 (b) $\sigma = 4.5$ μC/m^2, (c) $\sigma = 8.5$ μC/m^2, (d) $\sigma = 7.0$ μC/m^2, (e) $\sigma = 12$ μC/m^2, (f) $\sigma = 10$ μC/m^2.

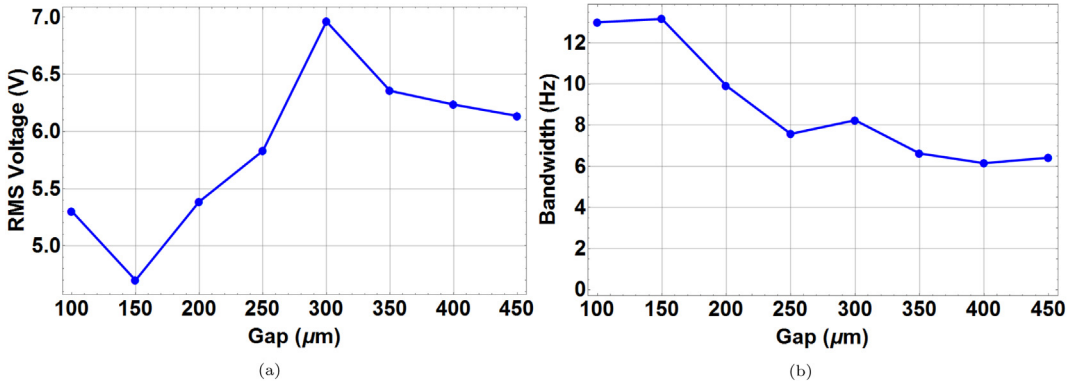

Fig. 11. (a) The output voltage as a function of the gap distance. Optimum gap found to be 300 μm (b) The measured bandwidth as a function of the gap distance. Optimum gap found to be around 150 μm.

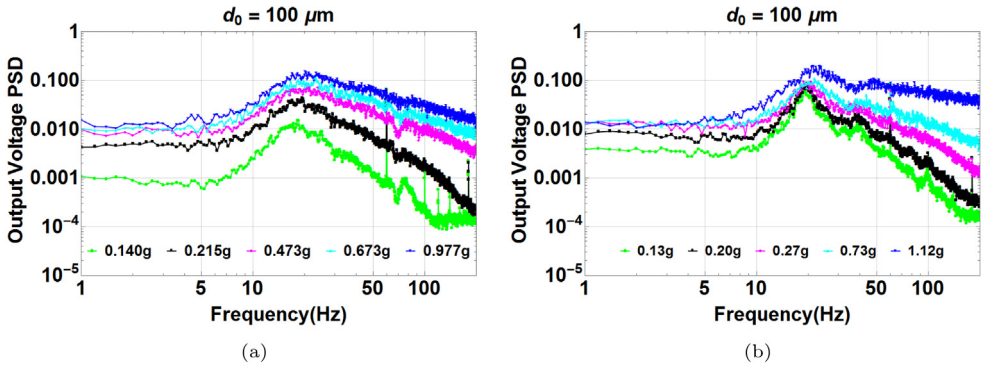

Fig. 12. Experimental PSD's for the output voltage of the triboelectric energy harvester under different RMS random signals.(a) The output voltage at a gap distance of 100 μm. (b) The output voltage at a gap distance of 250 μm.

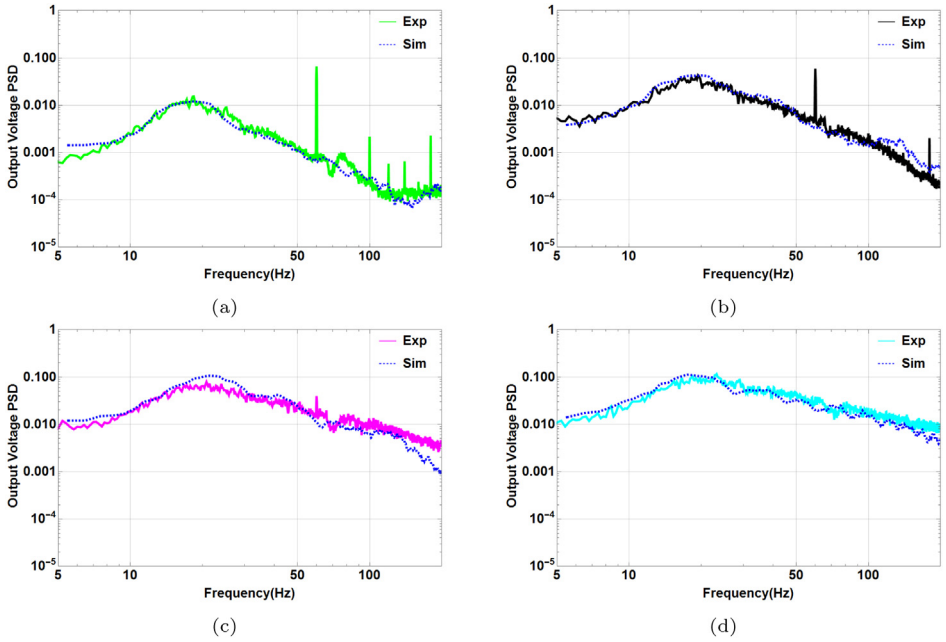

Fig. 13. Experimental and simulated PSD's for the output voltage of the triboelectric energy harvester at a gap distance of 100 μm, (a) 0.140 g RMS random signals and $\sigma = 0.05$ μC/m^2. (b) 0.215 g RMS random signals and $\sigma = 0.08$ μC/m^2 (c) 0.473 g RMS random signals and $\sigma = 0.1$ μC/m^2, (d) 0.673 g RMS random signals and $\sigma = 0.12$ μC/m^2.

Regardless of the low values of the generated power from the harmonic and random analysis, we demonstrated and provided a feasibility study that the triboelectricity is a viable energy harvesting technique that could be used with different applications undergoing types of excitations. Moreover, combining triboelectric energy harvester with impact vibration results in higher bandwidth. For future work, further analysis and optimization studies can be accomplished to achieve higher output power and significant improvement.

8. Conclusion

An impact triboelectric based energy harvester was proposed and fabricated. Also, a piecewise theoretical model was used to realize the contact and separation mechanisms of this harvester. The experimental results conducted under harmonic and random excitation for two different separation distances. A higher output voltage achieved by increasing the excitation acceleration. The maximum peak power density found to be 7 mW/m^2 at 1.4 g with an optimal load resistance of 4 $M\Omega$. The bandwidth increased by increasing the excitation amplitude caused by the contact-separation mechanism reaching a maximum value of 18 Hz at 1.4 g. The output voltage and bandwidth depend on the gap distance between the triboelectric layers. We noticed that large gap results in higher output voltage for low excitation amplitudes but with lower bandwidth. However, a small gap increases the frequency range of impact, and hence the bandwidth increases but with lower outputs. The simulated results were validated experimentally, and the results were in good agreement with each other. The model extended to validate our random excitation results, where the PSD results confirmed the results of harmonic excitation. Both experimental and simulated PSD results showed good agreements.

CRediT authorship contribution statement

Alwathiqbellah Ibrahim: Conception and design of study, Acquisition of data, Analysis and/or interpretation of data, Writing - original draft, Writing - review & editing. **Abdallah Ramini:** Acquisition of data, Analysis and/or interpretation of data, Writing - original draft, Writing - review & editing. **Shahrzad Towfighian:** Conception and design of study, Analysis and/or interpretation of data, Writing - original draft, Writing - review & editing.

Declaration of competing interest

The authors declare that they have no known competing financial interests or personal relationships that could have appeared to influence the work reported in this paper.

Acknowledgments

The authors are grateful for the generosity of Progressive Tools C. of Endwell, NY to provide the fabricated Al mold with micro-cylindrical patterns free of charge. All authors approved the version of the manuscript to be published.

Appendix

To solve the coupled dynamic equations (Eq. (1) and Eq. (2)), we use the shooting method as explained in Ref. Ibrahim et al. (2016), we let

$$\begin{aligned} X_1 &= y(t) \\ X_2 &= \dot{y}(t) \\ X_3 &= q(t) \end{aligned} \tag{A.1}$$

This will introduce the following three first order ordinary differential equations:

$$\begin{aligned} \dot{X}_1 &= X_2 \\ \dot{X}_1(t) &= \frac{1}{m}\begin{cases} -c_m X_2(t) - k_{eq} X_1(t) + \alpha X_3^2(t) - ma, & X_1(t) < g_i \\ -c_i X_2(t) - k_{eq} X_1(t) - k_i(X_1(t) - g_i) - ma, & X_1(t) \geq g_i \end{cases} \end{aligned} \tag{A.2}$$

$$\dot{X}_3(t) = -\beta X_3(t)\left(\frac{T}{\epsilon_r} + d_0 - X_1(t)\right) + \gamma\,(d_0 - X_1(t))$$

where α, β, and γ are parameters given by

$$\alpha = \frac{1}{2\epsilon_r \epsilon_0 S}, \quad \beta = \frac{1}{\epsilon_0 RS}, \quad \gamma = \frac{\sigma}{\epsilon_0 R} \tag{A.3}$$

The appropriate initial conditions that will give a periodic solution for the first order ode system are given by

$$\begin{aligned} y(0) &= X_1(0) = \eta_1 \\ \dot{y}(0) &= X_2(0) = \eta_2 \\ q(0) &= X_3(0) = \eta_3 \end{aligned} \tag{A.4}$$

Then we introduce new variables by taking the derivative of each variable, (X_1, X_2, X_3), with respect to the three initial conditions, (η_1, η_2, η_3)

$$\begin{aligned} &\frac{\partial X_1}{\partial \eta_1} = X_4, \quad \frac{\partial X_1}{\partial \eta_2} = X_5, \quad \frac{\partial X_1}{\partial \eta_3} = X_6 \\ &\frac{\partial X_2}{\partial \eta_1} = X_7, \quad \frac{\partial X_2}{\partial \eta_2} = X_8, \quad \frac{\partial X_2}{\partial \eta_3} = X_9 \\ &\frac{\partial X_3}{\partial \eta_1} = X_{10}, \quad \frac{\partial X_3}{\partial \eta_2} = X_{11}, \quad \frac{\partial X_3}{\partial \eta_3} = X_{12} \end{aligned} \tag{A.5}$$

Next, we take the time derivative for the previous system of equations

$$\begin{aligned} &\frac{\partial \dot{X}_1}{\partial \eta_1} = \dot{X}_4, \quad \frac{\partial \dot{X}_1}{\partial \eta_2} = \dot{X}_5, \quad \frac{\partial \dot{X}_1}{\partial \eta_3} = \dot{X}_6 \\ &\frac{\partial \dot{X}_2}{\partial \eta_1} = \dot{X}_7, \quad \frac{\partial \dot{X}_2}{\partial \eta_2} = \dot{X}_8, \quad \frac{\partial \dot{X}_2}{\partial \eta_3} = \dot{X}_9 \\ &\frac{\partial \dot{X}_3}{\partial \eta_1} = \dot{X}_{10}, \quad \frac{\partial \dot{X}_3}{\partial \eta_2} = \dot{X}_{11}, \quad \frac{\partial \dot{X}_3}{\partial \eta_3} = \dot{X}_{12} \end{aligned} \tag{A.6}$$

Using Eq. (A.5) and Eq. (A.6) we construct the first order ode system as given in Eq. (A.7) in Box I.

The initial conditions for the system above are given by:

$$\begin{aligned} X_1(0) &= \eta_{10} \\ X_2(0) &= \eta_{20} \\ X_3(0) &= \eta_{30} \\ X_4(0) &= \frac{\partial X_1(0)}{\partial \eta_1} = \frac{\partial \eta_1}{\partial \eta_1} = 1 \\ X_5(0) &= \frac{\partial X_1(0)}{\partial \eta_2} = \frac{\partial \eta_2}{\partial \eta_1} = 0 \\ X_6(0) &= \frac{\partial X_1(0)}{\partial \eta_3} = \frac{\partial \eta_3}{\partial \eta_1} = 0 \\ X_7(0) &= \frac{\partial X_2(0)}{\partial \eta_1} = \frac{\partial \eta_1}{\partial \eta_2} = 0 \\ X_8(0) &= \frac{\partial X_2(0)}{\partial \eta_2} = \frac{\partial \eta_2}{\partial \eta_2} = 1 \\ X_9(0) &= \frac{\partial X_2(0)}{\partial \eta_3} = \frac{\partial \eta_3}{\partial \eta_2} = 0 \\ X_{10}(0) &= \frac{\partial X_3(0)}{\partial \eta_1} = \frac{\partial \eta_1}{\partial \eta_3} = 0 \\ X_{11}(0) &= \frac{\partial X_3(0)}{\partial \eta_2} = \frac{\partial \eta_2}{\partial \eta_3} = 0 \\ X_{12}(0) &= \frac{\partial X_3(0)}{\partial \eta_3} = \frac{\partial \eta_3}{\partial \eta_3} = 1 \end{aligned} \tag{A.8}$$

where $(\eta_{10}, \eta_{20}, \eta_{30})$ are the initial guesses for the initial conditions that will lead to periodic solution. Integrate numerically Eqs. (A.3), (A.7), and (A.8) over one period T, $T = \frac{2\pi}{\Omega}$, where Ω is the excitation frequency. After that the values X_4 - X_{12} are calculated at time T, and the error in the initial conditions are calculated and updated by the following algebraic equation:

$$\begin{Bmatrix} \begin{pmatrix} X_4 & X_5 & X_6 \\ X_7 & X_8 & X_9 \\ X_{10} & X_{11} & X_{12} \end{pmatrix} - [I] \end{Bmatrix} \begin{Bmatrix} \partial\eta_1 \\ \partial\eta_2 \\ \partial\eta_3 \end{Bmatrix} = \begin{Bmatrix} \eta_{10} - X_1(T, \eta_{10}, \eta_{20}, \eta_{30}) \\ \eta_{20} - X_2(T, \eta_{10}, \eta_{20}, \eta_{30}) \\ \eta_{30} - X_3(T, \eta_{10}, \eta_{20}, \eta_{30}) \end{Bmatrix} \tag{A.9}$$

where, I is the Identity matrix, $(\partial\eta_1, \partial\eta_2, \partial\eta_3)$ are the errors in the initial conditions guesses. The process is repeated until convergence achieved and the errors are minimized.

$$
\begin{aligned}
\dot{X}_4 &= X_7 \\
\dot{X}_5 &= X_8 \\
\dot{X}_6 &= X_9 \\
\dot{X}_7 &= \frac{1}{m}\begin{cases} -c_m X_7(t) - k_{eq} X_4(t) + 2\alpha X_3(t) X_{10}(t), & X_1(t) < g_i \\ -c_i X_7(t) - (k_{eq} + k_i) X_4(t), & X_1(t) \geq g_i \end{cases} \\
\dot{X}_8 &= \frac{1}{m}\begin{cases} -c_m X_8(t) - k_{eq} X_5(t) + 2\alpha X_3(t) X_{11}(t), & X_1(t) < g_i \\ -c_i X_8(t) - (k_{eq} + k_i) X_5(t), & X_1(t) \geq g_i \end{cases} \\
\dot{X}_9 &= \frac{1}{m}\begin{cases} -c_m X_9(t) - k_{eq} X_6(t) + 2\alpha X_3(t) X_{12}(t), & X_1(t) < g_i \\ -c_i X_9(t) - (k_{eq} + k_i) X_6(t), & X_1(t) \geq g_i \end{cases} \\
\dot{X}_{10} &= -\beta X_{10}(t)\left(\frac{T}{\epsilon_r} + d_0 - X_1(t)\right) + \beta X_3(t) X_4(t) - \gamma X_4(t) \\
\dot{X}_{11} &= -\beta X_{11}(t)\left(\frac{T}{\epsilon_r} + d_0 - X_1(t)\right) + \beta X_3(t) X_5(t) - \gamma X_5(t) \\
\dot{X}_{12} &= -\beta X_{12}(t)\left(\frac{T}{\epsilon_r} + d_0 - X_1(t)\right) + \beta X_3(t) X_6(t) - \gamma X_6(t)
\end{aligned}
\tag{A.7}
$$

Box I.

References

Adhikari, S., Friswell, M., Inman, D., 2009. Piezoelectric energy harvesting from broadband random vibrations. Smart Mater. Struct. 18 (11), 115005.

Ahmadian, M., 2008. Active and Passive Smart Structures and Integrated Systems 2008. SPIE.

Al-Ashtari, W., Hunstig, M., Hemsel, T., Sextro, W., 2013. Enhanced energy harvesting using multiple piezoelectric elements: theory and experiments. Sensors Actuators A 200, 138–146.

Bilgen, O., Friswell, M.I., Ali, S.F., Litak, G., 2015. Broadband vibration energy harvesting from a vertical cantilever piezocomposite beam with tip mass. Int. J. Struct. Stab. Dyn. 15 (02), 1450038.

Blystad, L.-C.J., Halvorsen, E., Husa, S., 2010. Piezoelectric MEMS energy harvesting systems driven by harmonic and random vibrations. IEEE Trans. Ultrason. Ferroelectr. Freq. Control 57 (4).

Chen, C., Chen, L., Wu, Z., Guo, H., Yu, W., Du, Z., Wang, Z.L., 2020. 3D double-faced interlock fabric triboelectric nanogenerator for bio-motion energy harvesting and as self-powered stretching and 3D tactile sensors. Mater. Today 32, 84–93.

Chen, J., Yang, J., Guo, H., Li, Z., Zheng, L., Su, Y., Wen, Z., Fan, X., Wang, Z.L., 2015. Automatic mode transition enabled robust triboelectric nanogenerators. ACS Nano 9 (12), 12334–12343.

Cottone, F., Gammaitoni, L., Vocca, H., Ferrari, M., Ferrari, V., 2012. Piezoelectric buckled beams for random vibration energy harvesting. Smart Mater. Struct. 21 (3), 035021.

Dhakar, L., Liu, H., Tay, F., Lee, C., 2013. A new energy harvester design for high power output at low frequencies. Sensors Actuators A 199, 344–352.

Dhakar, L., Pitchappa, P., Tay, F.E.H., Lee, C., 2016. An intelligent skin based self-powered finger motion sensor integrated with triboelectric nanogenerator. Nano Energy 19, 532–540.

Dhakar, L., Tay, F., Lee, C., 2014. Investigation of contact electrification based broadband energy harvesting mechanism using elastic PDMS microstructures. J. Micromech. Microeng. 24 (10), 104002.

Dhakar, L., Tay, F., Lee, C., 2015a. Broadband vibration energy harvesting using triboelectric mechanism. In: International Conference on Experimental Mechanics 2014. International Society for Optics and Photonics, p. 93021H.

Dhakar, L., Tay, F.E.H., Lee, C., 2015b. Development of a broadband triboelectric energy harvester with SU-8 micropillars. J. Microelectromech. Syst. 24 (1), 91–99.

Diaz, A., Felix-Navarro, R., 2004. A semi-quantitative tribo-electric series for polymeric materials: The influence of chemical structure and properties. J. Electrost. 62 (4), 277–290.

Dong, K., Deng, J., Ding, W., Wang, A.C., Wang, P., Cheng, C., Wang, Y.-C., Jin, L., Gu, B., Sun, B., et al., 2018. Versatile core–sheath yarn for sustainable biomechanical energy harvesting and real-time human-interactive sensing. Adv. Energy Mater. 8 (23), 1801114.

Erturk, A., Hoffmann, J., Inman, D., 2009. A piezomagnetoelastic structure for broadband vibration energy harvesting. Appl. Phys. Lett. 94 (25), 254102.

Fan, F.-R., Tian, Z.-Q., Wang, Z.L., 2012. Flexible triboelectric generator. Nano Energy 1 (2), 328–334.

Ferrari, M., Bau, M., Guizzetti, M., Ferrari, V., 2011. A single-magnet nonlinear piezoelectric converter for enhanced energy harvesting from random vibrations. Sensors Actuators A 172 (1), 287–292.

Gammaitoni, L., Neri, I., Vocca, H., 2009. Nonlinear oscillators for vibration energy harvesting. Appl. Phys. Lett. 94 (16), 164102.

Guo, T., Liu, G., Pang, Y., Wu, B., Xi, F., Zhao, J., Bu, T., Fu, X., Li, X., Zhang, C., et al., 2018a. Compressible hexagonal-structured triboelectric nanogenerators for harvesting tire rotation energy. Extreme Mech. Lett. 18, 1–8.

Guo, X., Zhang, Y., Fan, K., Lee, C., Wang, F., 2020. A comprehensive study of non-linear air damping and "pull-in" effects on the electrostatic energy harvesters. Energy Convers. Manage. 203, 112264.

Guo, T., Zhao, J., Liu, W., Liu, G., Pang, Y., Bu, T., Xi, F., Zhang, C., Li, X., 2018b. Self-powered hall vehicle sensors based on triboelectric nanogenerators. Adv. Mater. Technol. 3 (8), 1800140.

Gupta, R.K., Shi, Q., Dhakar, L., Wang, T., Heng, C.H., Lee, C., 2017. Broadband energy harvester using non-linear polymer spring and electromagnetic/triboelectric hybrid mechanism. Sci. Rep. 7, 41396.

Halvorsen, E., 2008. Energy harvesters driven by broadband random vibrations. J. Microelectromech. Syst. 17 (5), 1061–1071.

Henniker, J., 1962. Triboelectricity in Polymers. Nature Publishing Group.

Ibrahim, A., Towfighian, S., Younis, M.I., 2017. Dynamics of transition regime in bistable vibration energy harvesters. J. Vib. Acoust. 139 (5), 051008.

Ibrahim, A., Towfighian, S., Younis, M., Su, Q., 2016. Magnetoelastic beam with extended polymer for low frequency vibration energy harvesting. In: SPIE Smart Structures and Materials+ Nondestructive Evaluation and Health Monitoring. International Society for Optics and Photonics, p. 98060B.

Jin, L., Deng, W., Su, Y., Xu, Z., Meng, H., Wang, B., Zhang, H., Zhang, B., Zhang, L., Xiao, X., et al., 2017. Self-powered wireless smart sensor based on maglev porous nanogenerator for train monitoring system. Nano Energy 38, 185–192.

Jin, C., Kia, D.S., Jones, M., Towfighian, S., 2016. On the contact behavior of micro-/nano-structured interface used in vertical-contact-mode triboelectric nanogenerators. Nano Energy 27, 68–77.

Khan, U., Kim, T.-H., Ryu, H., Seung, W., Kim, S.-W., 2017. Graphene tribotronics for electronic skin and touch screen applications. Adv. Mater. 29 (1), 1603544.
Lefeuvre, E., Badel, A., Richard, C., Guyomar, D., 2007. Energy harvesting using piezoelectric materials: case of random vibrations. J. Electroceram. 19 (4), 349–355.
Li, S., Crovetto, A., Peng, Z., Zhang, A., Hansen, O., Wang, M., Li, X., Wang, F., 2016a. Bi-resonant structure with piezoelectric PVDF films for energy harvesting from random vibration sources at low frequency. Sensors Actuators A 247, 547–554.
Li, X., Lin, Z.-H., Cheng, G., Wen, X., Liu, Y., Niu, S., Wang, Z.L., 2014. 3D fiber-based hybrid nanogenerator for energy harvesting and as a self-powered pressure sensor. ACS Nano 8 (10), 10674–10681.
Li, S., Peng, Z., Zhang, A., Luo, D., Wang, F., 2016b. Dual resonant structure for energy harvesting from random vibration sources. In: 2016 IEEE 11th Annual International Conference on Nano/Micro Engineered and Molecular Systems (NEMS). IEEE, pp. 255–259.
Li, X., Tao, J., Wang, X., Zhu, J., Pan, C., Wang, Z.L., 2018. Networks of high performance triboelectric nanogenerators based on liquid–solid interface contact electrification for harvesting low-frequency blue energy. Adv. Energy Mater. 8 (21), 1800705.
Litak, G., Friswell, M., Adhikari, S., 2010. Magnetopiezoelastic energy harvesting driven by random excitations. Appl. Phys. Lett. 96 (21), 214103.
Liu, H., Lee, C., Kobayashi, T., Tay, C.J., Quan, C., 2012. Piezoelectric MEMS-based wideband energy harvesting systems using a frequency-up-conversion cantilever stopper. Sensors Actuators A 186, 242–248.
Liu, M., Pu, X., Jiang, C., Liu, T., Huang, X., Chen, L., Du, C., Sun, J., Hu, W., Wang, Z.L., 2017. Large-area all-textile pressure sensors for monitoring human motion and physiological signals. Adv. Mater. 29 (41), 1703700.
Liu, H., Zhong, J., Lee, C., Lee, S.-W., Lin, L., 2018. A comprehensive review on piezoelectric energy harvesting technology: materials, mechanisms, and applications. Appl. Phys. Rev. 5 (4), 041306.
Mahmoud, M.A.E., 2010. Switchless Electrostatic Vibration Micro-Power Generators. (Ph.D. thesis). University of Waterloo.
Mann, B., Sims, N., 2009. Energy harvesting from the nonlinear oscillations of magnetic levitation. J. Sound Vib. 319 (1), 515–530.
Masana, R., Daqaq, M.F., 2011. Electromechanical modeling and nonlinear analysis of axially loaded energy harvesters. J. Vib. Acoust. 133 (1), 011007.
Meng, X., Cheng, Q., Jiang, X., Fang, Z., Chen, X., Li, S., Li, C., Sun, C., Wang, W., Wang, Z.L., 2018. Triboelectric nanogenerator as a highly sensitive self-powered sensor for driver behavior monitoring. Nano Energy 51, 721–727.
Nguyen, S.D., Halvorsen, E., 2011. Nonlinear springs for bandwidth-tolerant vibration energy harvesting. J. Microelectromech. Syst. 20 (6), 1225–1227.
NI, 1976. Labview'.
Niu, S., Wang, S., Lin, L., Liu, Y., Zhou, Y.S., Hu, Y., Wang, Z.L., 2013. Theoretical study of contact-mode triboelectric nanogenerators as an effective power source. Energy Environ. Sci. 6 (12), 3576–3583.
Papoulis, A., Pillai, S., 2002. Probability, Random Variables, and Stochastic Processes. Tata McGraw-Hill Education.
2015. Progressive tool co kernel description. http://www.progressivetool.com/. (Accessed 30 September 2015).
Sari, I., Balkan, T., Kulah, H., 2008. An electromagnetic micro power generator for wideband environmental vibrations. Sensors Actuators A 145, 405–413.
Shen, Q., Xie, X., Peng, M., Sun, N., Shao, H., Zheng, H., Wen, Z., Sun, X., 2018. Self-powered vehicle emission testing system based on coupling of triboelectric and chemoresistive effects. Adv. Funct. Mater. 28 (10), 1703420.
Shi, Q., He, T., Lee, C., 2019. More than energy harvesting–Combining triboelectric nanogenerator and flexible electronics technology for enabling novel micro-/nano-systems. Nano Energy 57, 851–871.
Sneller, A., Cette, P., Mann, B., 2011. Experimental investigation of a post-buckled piezoelectric beam with an attached central mass used to harvest energy. Proc. Inst. Mech. Eng. I: J. Syst. Control Eng. 225 (4), 497–509.
Soliman, M., Abdel-Rahman, E., El-Saadany, E., Mansour, R., 2008. A wideband vibration-based energy harvester. J. Micromech. Microeng. 18 (11), 115021.
Soliman, M.S., Abdel-Rahman, E.M., El-Saadany, E.F., Mansour, R.R., 2009. A design procedure for wideband micropower generators. J. Microelectromech. Syst. 18 (6), 1288–1299.
Stanton, S.C., McGehee, C.C., Mann, B.P., 2010. Nonlinear dynamics for broadband energy harvesting: Investigation of a bistable piezoelectric inertial generator. Physica D 239 (10), 640–653.
Stanton, S.C., Owens, B.A., Mann, B.P., 2012. Harmonic balance analysis of the bistable piezoelectric inertial generator. J. Sound Vib. 331 (15), 3617–3627.
Wang, Z.L., 2013. Triboelectric nanogenerators as new energy technology for self-powered systems and as active mechanical and chemical sensors. ACS Nano 7 (11), 9533–9557.
Wang, Z.L., Jiang, T., Xu, L., 2017a. Toward the blue energy dream by triboelectric nanogenerator networks. Nano Energy 39, 9–23.
Wang, X., Niu, S., Yin, Y., Yi, F., You, Z., Wang, Z.L., 2015. Triboelectric nanogenerator based on fully enclosed rolling spherical structure for harvesting low-frequency water wave energy. Adv. Energy Mater. 5 (24).
Wang, Z.L., Wu, W., 2012. Nanotechnology-enabled energy harvesting for self-powered micro-/nanosystems. Angew. Chem., Int. Ed. Engl. 51 (47), 11700–11721.
Wang, J., Zhang, H., Xie, Y., Yan, Z., Yuan, Y., Huang, L., Cui, X., Gao, M., Su, Y., Yang, W., et al., 2017b. Smart network node based on hybrid nanogenerator for self-powered multifunctional sensing. Nano Energy 33, 418–426.
Wen, Z., Yeh, M.-H., Guo, H., Wang, J., Zi, Y., Xu, W., Deng, J., Zhu, L., Wang, X., Hu, C., et al., 2016. Self-powered textile for wearable electronics by hybridizing fiber-shaped nanogenerators, solar cells, and supercapacitors. Sci. Adv. 2 (10), e1600097.
Wolfram, S., 1987. Mathematica'.
Yang, Y., Sun, N., Wen, Z., Cheng, P., Zheng, H., Shao, H., Xia, Y., Chen, C., Lan, H., Xie, X., et al., 2018. Liquid-metal-based super-stretchable and structure-designable triboelectric nanogenerator for wearable electronics. Acs Nano 12 (2), 2027–2034.
Yang, W., Towfighian, S., 2017. A hybrid nonlinear vibration energy harvester. Mech. Syst. Signal Process. 90, 317–333.
Yi, F., Lin, L., Niu, S., Yang, P.K., Wang, Z., Chen, J., Zhou, Y., Zi, Y., Wang, J., Liao, Q., et al., 2015. Stretchable-rubber-based triboelectric nanogenerator and its application as self-powered body motion sensors. Adv. Funct. Mater. 25 (24), 3688–3696.
Zeng, W., Tao, X.-M., Chen, S., Shang, S., Chan, H.L.W., Choy, S.H., 2013. Highly durable all-fiber nanogenerator for mechanical energy harvesting. Energy Environ. Sci. 6 (9), 2631–2638.
Zhang, X.-S., Han, M.-D., Wang, R.-X., Meng, B., Zhu, F.-Y., Sun, X.-M., Hu, W., Wang, W., Li, Z.-H., Zhang, H.-X., 2014. High-performance triboelectric nanogenerator with enhanced energy density based on single-step fluorocarbon plasma treatment. Nano Energy 4, 123–131.
Zhang, Y., Wang, T., Luo, A., Hu, Y., Li, X., Wang, F., 2018. Micro electrostatic energy harvester with both broad bandwidth and high normalized power density. Appl. Energy 212, 362–371.
Zhang, Y., Wang, T., Zhang, A., Peng, Z., Luo, D., Chen, R., Wang, F., 2016. Electrostatic energy harvesting device with dual resonant structure for wideband random vibration sources at low frequency. Rev. Sci. Instrum. 87 (12), 125001.
Zhao, S., Erturk, A., 2012. Electroelastic modeling and experimental validations of piezoelectric energy harvesting from broadband random vibrations of cantilevered bimorphs. Smart Mater. Struct. 22 (1), 015002.
Zheng, Q., Zou, Y., Zhang, Y., Liu, Z., Shi, B., Wang, X., Jin, Y., Ouyang, H., Li, Z., Wang, Z.L., 2016. Biodegradable triboelectric nanogenerator as a life-time designed implantable power source. Science Adv. 2 (3), e1501478.
Zhou, T., Zhang, C., Han, C.B., Fan, F.R., Tang, W., Wang, Z.L., 2014. Woven structured triboelectric nanogenerator for wearable devices. ACS Appl. Mater. Interfaces 6 (16), 14695–14701.
Zi, Y., Wang, J., Wang, S., Li, S., Wen, Z., Guo, H., Wang, Z.L., 2016. Effective energy storage from a triboelectric nanogenerator. Nat. Commun. 7.